NANO LETTERS

pubs.acs.org/NanoLett

Letter

Resonant Plasmonic–Biomolecular Chiral Interactions in the Far-Ultraviolet: Enantiomeric Discrimination of sub-10 nm Amino Acid Films

Tiago Ramos Leite, Lin Zschiedrich, Orhan Kizilkaya, and Kevin M. McPeak*

Cite This: *Nano Lett.* 2022, 22, 7343–7350

Read Online

ACCESS | Metrics & More | Article Recommendations | Supporting Information

ABSTRACT: Resonant plasmonic–molecular chiral interactions are a promising route to enhanced biosensing. However, biomolecular optical activity primarily exists in the far-ultraviolet regime, posing significant challenges for spectral overlap with current nano-optical platforms. We demonstrate experimentally and computationally the enhanced chiral sensing of a resonant plasmonic–biomolecular system operating in the far-UV. We develop a full-wave model of biomolecular films on Al gammadion arrays using experimentally derived chirality parameters. Our calculations show that detectable enhancements in the chiroptical signals from small amounts of biomolecules are possible only when tight spectral overlap exists between the plasmonic and biomolecular chiral responses. We support this conclusion experimentally by using Al gammadion arrays to enantiomerically discriminate ultrathin (<10 nm thick) films of tyrosine. Notably, the chiroptical signals of the bare films were within instrumental noise. Our results demonstrate the importance of using far-UV active metasurfaces for enhancing natural optical activity.

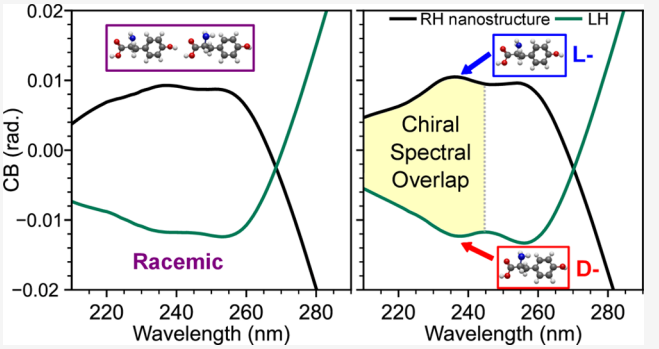

KEYWORDS: *ultraviolet plasmonics, chiral sensing, biosensing, optical activity, enantiomeric discrimination*

Since the seminal works on optical chirality and superchiral light by Tang and Cohen,[1,2] researchers have employed a myriad of nano-optics approaches aimed at amplifying the intrinsically small effects[1,3] of natural optical activity (OA)—circular dichroism (CD) and birefringence (CB).[4] Nanostructures can create electromagnetic near-fields with optical chirality density higher than circularly polarized light (CPL),[5] thus increasing the CD from chiral molecules in these locations.[1] Initially, most nano-optics studies consisted of plasmonic nanoparticles and nanoarrays.[6] More recently, there has been growing interest in developing[7] chiroptical dielectric platforms,[8−11] owning in part to their ability to sustain both electric and magnetic resonances, which, when properly coupled, can lead to high optical chirality densities.[12] Unfortunately, these resonances mainly arise in the visible to the infrared (IR), leading to great spectral mismatches with natural OA.[7] Most chiral analytes of interest (such as biomolecules) have absorption bands in the ultraviolet (UV).[13] In this context, low-loss, high-index dielectric materials are still limited for the UV region,[14−16] especially in the far-UV regime (λ < 250 nm) where CD signals are used to assess biomolecular structure.[13]

As for plasmonics, achiral nanostructures have been the most thoroughly investigated.[17] Assembling achiral metallic nanoparticles into chiral superstructures[18−23] can lead to strong CD signals from dipole–dipole interactions among neighboring particles.[24] Furthermore, the presence of chiral molecules close to achiral metallic nanostructures can induce chiroptical signals at the plasmon frequency.[25−29] The use of achiral nanostructures is motivated by a desire to avoid the strong CD signals from their chiral counterparts which could overshadow the weak molecular chiroptical response[7,17,30−33] or require data postprocessing to assess the chiral analyte signal.[10,17,32] Conversely, chiral plasmonic nanostructures can generate high optical chirality in their near-fields.[5,7,33,34] Previous works which utilized chiral plasmonic metasurfaces relied on the differences in the spectral shift induced by a chiral analyte when interacting with a pair of enantiomeric arrays[35,36] or on the sum of the plasmonic chiroptical signal in the presence and absence of the chiral analyte.[37] The drawback of these approaches is that nanofabrication heterogeneities[32] can perturb the perfectly mirror-symmetric spectrum of the

Received: April 28, 2022
Revised: September 6, 2022
Published: September 9, 2022

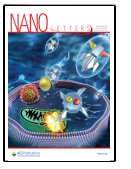

https://doi.org/10.1021/acs.nanolett.2c01724
Nano Lett. 2022, 22, 7343−7350

enantiomorph arrays. Furthermore, regardless of the platform, the energy mismatch between natural optical activity and metamaterial resonances remains the most significant obstacle for chiral sensing.[33]

The benefits of overlapping molecular OA and achiral nano-optical resonances were previously studied.[11,38−40] Notably, detuning of the molecular and plasmonic resonances was detrimental to the observed CD signals.[38,40] Experimentally,[11,40] the evaluation of these resonant interactions was permitted by conjugating DNA to chromophores, where an induced OA in the visible was enabled by the chiral macromolecule.[41,42] Therefore, the natural OA of the DNA molecule was not directly assessed. In this work, we study the resonant chiral interactions between biomolecules and plasmonic near-fields in the far-UV by means of electromagnetic calculations and experiments. To the best of our knowledge, this is the first time a platform enabling spectral overlap between biomolecular and plasmonic chiral resonances is used to assess natural OA directly. We determine the handedness of the analyte by analyzing the fingerprint-like chiral signature of the plasmonic−biomolecular system. Our biosensing scheme enables the enantiomeric discrimination of ultrathin (<10 nm thick) amino acid films. Notably, the CB signal of the bare biomolecular films could not be reliably resolved by our instrument. Our work provides a critical step forward in understanding resonant plasmonic−biomolecular interactions and developing metasurfaces for enhanced chiral biosensing.

Aluminum is a promising metal for UV plasmonics,[43−45] displaying excellent optical properties in the UV, especially when low base pressures and fast deposition rates are employed.[46] Additionally, its passivating oxide layer promotes the stability of Al nanostructures to air and organic solvents.[47]

To better understand resonant plasmonic−biomolecular chiral−chiral interactions, we start by performing full-wave electromagnetic (EM) simulations of Al gammadion arrays coated with 20 nm thick achiral and chiral biomolecular films (Figure 1a). The latter were implemented in the finite-element solver JCMsuite (JCMwave GmbH, Germany) with bi-isotropic constitutive relations[48,49] and initially modeled as a homogeneous material with index of refraction n = 2.045 + 0.230i, and chirality parameter κ = 0.004 or 0.004i. For purely real (Im{κ} = 0) and imaginary (Re{κ} = 0) chirality parameters, the film only displays CB and CD, respectively[50−52] (Figure 1b). To verify the effects of the chiral medium on the plasmonic−biomolecular system, we use as reference the chiroptical signals of the nanostructures coated with a racemic film,[32] which exhibit no net chirality, i.e., κ = 0. The nanostructures had a total thickness of 105 nm (5 nm Ti and 100 nm Al) and were on top of a fused-silica substrate (see Figure S1 for dimensions).

As expected, when the right- (RH, solid line) and left-handed (LH, dashed line) gammadion arrays are coated by racemic layers (black curves), their CD (Figure 1c) and CB (Figure 1d) spectra are mirror images of each other. The effects of the biomolecular chirality are displayed in the orange and blue curves of Figure 1c,d. Notice that we subtracted the CD and CB signals arising from the isolated 20 nm biomolecular films from the relevant spectra presented in Figure 1c,d, respectively. These plots show that the mirror symmetry among the chiroptical signals of the coated RH and LH gammadions is broken when the molecular film is chiral. These changes are most noticeably near the crossing point of

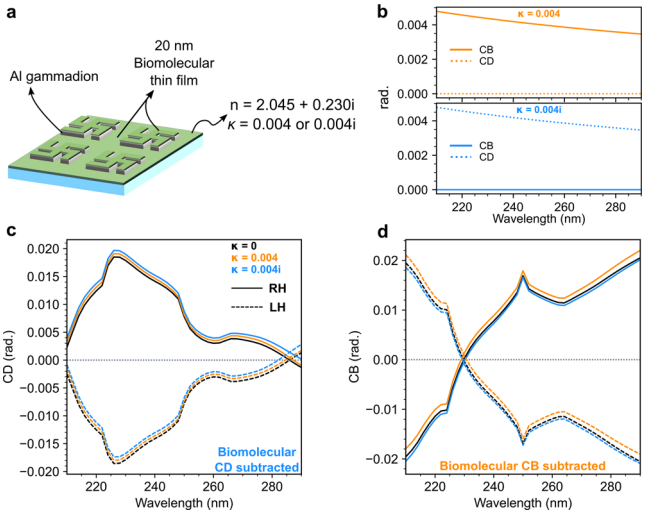

Figure 1. Simulated far-field optical response of the UV plasmonic−biomolecular chiral system. (a) Schematic of a LH Al gammadion array coated with 20 nm of biomolecular layers, which we initially model with constant optical properties. (b) For chirality parameters κ = 0.004 and 0.004i, the molecular layers display only CB and CD, respectively. (c, d) Effects of biomolecular chirality on the plasmonic chiroptical response. When the films are racemic, i.e., achiral, the (c) CD and (d) CB signals of the RH (solid black) and LH (dashed black) gammadions display the expected mirror symmetry. Conversely, when the films are chiral, this mirror symmetry is perturbed. In panel c, even though the biomolecular κ is purely real, it asymmetrically affects the CD of the system when it is composed of RH (solid orange) and LH (dashed orange) gammadions. The lack of mirror symmetry is more pronounced when Im{κ} ≠ 0, i.e., when both biomolecules and plasmonic structure have a CD response (solid and dashed blue lines). Note here that we subtracted the CD signal arising from the bare biomolecular film (the observed differences are not simply an additive effect). For panel d, the same remarks are also valid for the CB signal of the plasmonic−biomolecular system.

the two enantiomers, i.e., at 285 nm for Figure 1c and at 230 nm for Figure 1d. In Figure 1c, even though the chiral medium has no CD of its own, it asymmetrically perturbs the electromagnetic response of the RH (solid orange) and LH (dashed orange) nanostructures to CPL. Re{κ} can modify the CD response of plasmonic−biomolecular systems.[53] When the film has a purely imaginary κ, the lack of mirror symmetry is more substantial (Figure 1c, blue curves), even after considering the background biomolecular chiroptical signal. The same observations are valid for the CB signals (Figure 1d). For real biomolecules, with dispersive n and κ, we expect to see the largest deviations from the reference spectra, when the CD (or CB) response of the plasmonic nanostructure spectrally overlaps with the respective chiral signal of the biomolecule. Recently, Both et al.[53] theoretically described the multiple mechanisms contributing to the CD signal of chiral plasmonic nanostructures interacting with a chiral medium. We expect the same effects to be present in our work because both nanostructure and biomolecular films are chiral. An exhaustive mechanistic evaluation is, however, beyond the scope of this work.

To better understand our resonant plasmonic−biomolecular system, we modified our simulation to account for dispersion in the chiral parameter of real materials, using tyrosine (Tyr) as our model biomolecule. We extracted Im{κ} from the CD and Re{κ} from the CB signal of a 90 nm thin film of L-Tyr on top

https://doi.org/10.1021/acs.nanolett.2c01724
Nano Lett. 2022, 22, 7343−7350

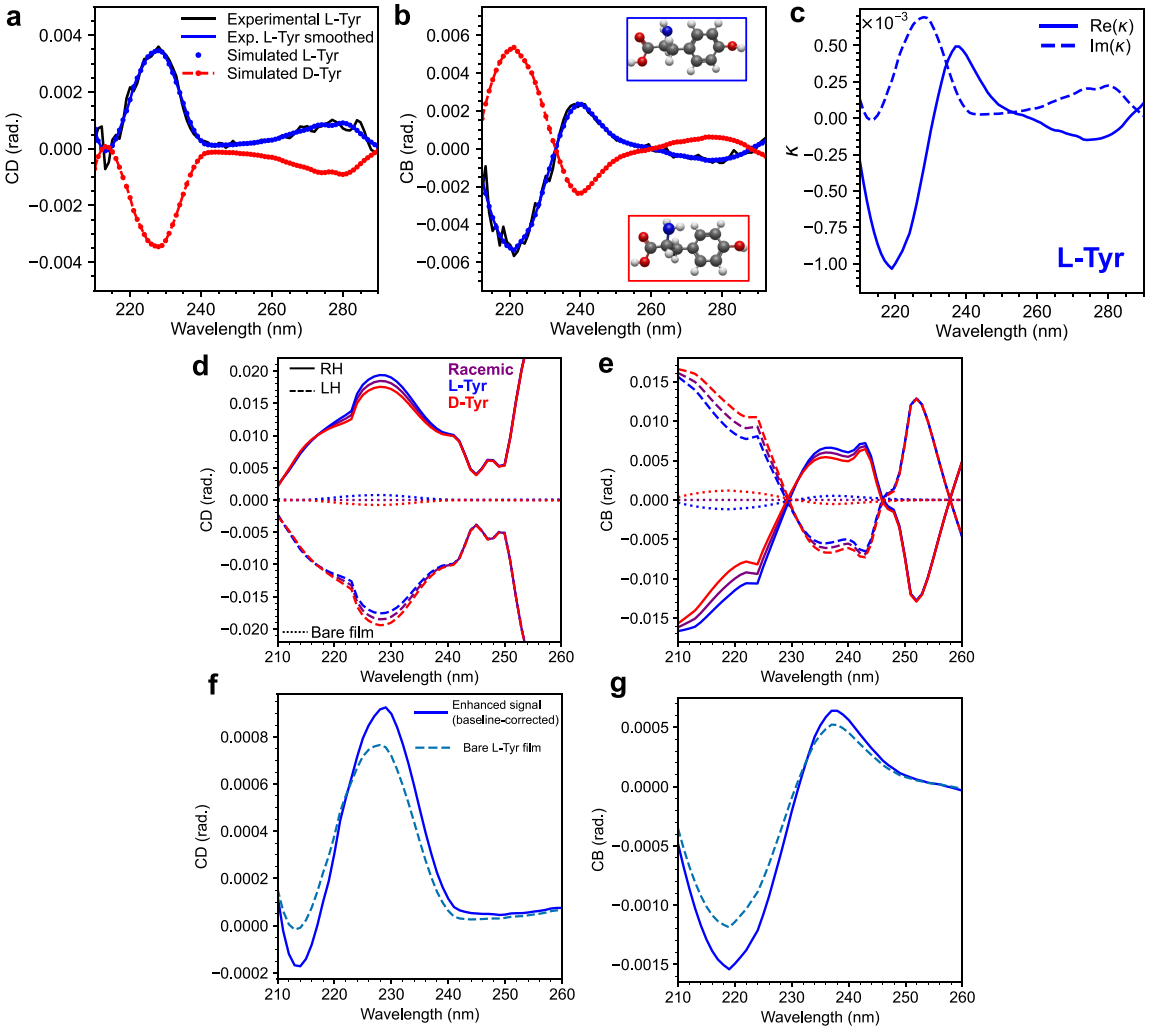

Figure 2. Far-field simulations of a resonant plasmonic−biomolecular system with real-world chirality parameter (κ). We employed tyrosine as our model biomolecule. Experimental and numerical (a) CD and (b) CB of a 90 nm thick L-Tyr film on top of a fused-silica substrate. The experimental CB and CD signals of the film were used to retrieve (c) Re{κ} and Im{κ} for L-Tyr, respectively. To simulate D-Tyr, we simply flipped the sign of κ determined for the L-enantiomer. (d) CD spectra of bare films (dotted lines) and of RH (solid lines) and LH (dashed lines) gammadion arrays coated with rac-Tyr (purple curves), L-Tyr (blue curves), and D-Tyr (red curves). We use as reference the CD spectrum of the arrays coated with racemic layers, which form a perfect mirror image. Dissimilarly, when the plasmonic−molecular system is composed of chiral films, the CD spectra of the gammadion enantiomorphs lose this symmetry. Compared to when it is coated with a racemic film, a given gammadion enantiomer will interact differently with L- and D-Tyr. (f, g) For the RH gammadion coated with L-Tyr, baseline-correction procedure performed to remove the bare signal of the plasmonic nanostructure. The baseline-corrected (f) CD and (g) CB are larger than the signals of the bare film, which clearly indicate enhancement.

of a fused-silica substrate. Panels a and b of Figure 2 display the experimental and numerical values for CD and CB, respectively (see Methods in the Supporting Information for details). To simulate D-Tyr, we flipped the sign of κ determined for the L-enantiomer. We note that, at resonance (Figure 2c), the highest absolute values for Re{κ} and Im{κ} of L-Tyr are approximately 1×10^{-3} and 7×10^{-4}, respectively (see Supporting Information for tabulated data). At 310 nm, which is still close to the resonant frequencies, Re{κ} quickly decays to $\sim 4 \times 10^{-5}$, and additionally, the film is essentially transparent, i.e., Im{n} = 0 (Figure S3). We observe the same effects for the amino acid Tryptophan (Trp); see Figure S4. Aromatic amino acid (such as Tyr and Trp) side chains contribute[54] and influence[54,55] the CD spectrum of proteins. Therefore, if one aims to sense the chirality of small amounts of biomolecules, it is paramount that the metasurface is active in the far-UV spectrum region.[33]

In Figure 2d,e, we present the CD and CB spectra of the RH (solid) and LH (dashed) gammadions coated with racemic tyrosine (purple; rac-Tyr) and L- (blue) and D-Tyr (red). The dotted curves represent the chiroptical signal of the bare amino acid film. Like in the previous simulation (Figure 1c,d), the reference consists of the chiroptical response from the Al gammadions surrounded by racemic layers. When the nanostructures are coated with L- or D-Tyr, the mirror symmetry among the CD and CB signals of the gammadion enantiomorphs are perturbed. For a fixed-handedness of gammadion (e.g., RH), the concavities of the CD spectra in the region $210 \leq \lambda \leq 220$ nm are altered with respect to the reference. Furthermore, the peak at around $\lambda \approx 228$ nm is increased or decreased depending on the combination of chiral Tyr and gammadion enantiomers. Because of symmetry, the CD and CB signals for the pair L-Tyr-RH-gammadion and D-Tyr-LH-gammadion are mirror-symmetric to one another

https://doi.org/10.1021/acs.nanolett.2c01724
Nano Lett. 2022, 22, 7343−7350

(holding also for L-Tyr-LH-gammadion and D-Tyr-RH-gammadion). Similar findings are also present in the CB signals (Figure 2e). This can be a mechanism used for the enantiomeric discrimination of the analyte.

These observed effects are more pronounced in the regions where the amino acids have stronger OA. At longer wavelengths, where biomolecular OA is vanishing, the mirror symmetry between the chiroptical signals of RH and LH gammadion arrays essentially reemerges (Figure 2d,e for $\lambda >$ 250 nm and Figure S5). Previous works[38,56] have studied the resonant interaction of achiral nanoparticles with chiral molecules in the visible range. They verified that driving a plasmonic−molecular system out of resonance had detrimental effects to the observed CD enhancements. Our computational results suggest that when chiral nanostructures are involved, a resonant system with good spectral overlap is likewise important for superior chiral biosensing.

Given that the chiral nanostructure exhibits CD and CB signals of its own, we performed a baseline correction method[57] to take into consideration the "background" chiroptical response of the gammadion. In Figure 2f, we present the results of this procedure for the RH gammadion coated with L-Tyr, where $CD_{baseline\text{-}corrected}$ = $CD_{RH\text{-}gammadion\text{-}L\text{-}Tyr}$ − $CD_{RH\text{-}gammadion\text{-}rac\text{-}Tyr}$; in addition to the CD signal of the bare L-Tyr film (20 nm on top of a fused-silica substrate). Clearly, the overall CD is boosted in comparison to the isolated amino acid film. In Figure 2g, the same procedure also reveals an overall enhancement for the CB signal. We posit that the enhancement is due to resonant chiral plasmonic−molecular near-field interactions.

To test this hypothesis, we performed simulations of the RH gammadion with 20 nm of the L-Tyr film on top. We varied the dimensions (e.g., arm width and pitch) of the RH gammadion and calculated the impact on the $CD_{baseline\text{-}corrected}$ signal (see Figure S6). Our simulations confirm that spectral overlap between plasmonic and biomolecular resonances is of great importance. When we increased the number of gammadions (145 nm arm width) in a fixed space by reducing its pitch from 500 to 475 nm, the signal enhancement was not increased given that the system was driven off-resonance. Negligible enhancements were observed for the array with 550 nm pitch regardless of the nanostructure dimensions due to a lack of plasmonic OA at ∼228 nm, i.e., where the L-Tyr films exhibit OA. Overall, the L-Tyr CD signal was only enhanced when the system displayed a clear spectral overlap between biomolecular and plasmonic OA resonances. The net OA enhancement can arise due to multiple mechanisms, among them are resonance shifts and modifications in the excitation and emission of the resonator modes.[53] These individual calculations are, however, beyond the scope of this work.

We then investigated the near-fields of the gammadions. Chiral plasmonic nanostructures generate electromagnetic fields with enhanced optical chirality ($C_{enh} = C/|C_{CPL}|$),[5] i.e., "superchiral fields",[1,2] where the optical chirality density is higher than that for CPL ($|C_{enh}| > 1$). We illuminate the nanostructure with circular polarization of negative (e^-) and positive (e^+) ellipticities at λ = 228 nm; C_{enh} is computed only in regions accessible by the biomolecules. Figure 3a displays the side view of a LH gammadion array coated with 20 nm of rac-Tyr; two reference points are also provided. In Figure 3b, we present C_{enh} plots for a *xz*-cut at the middle of the unit cell. Panels c and d of Figure 3 show *xy*-plots of a 5 nm-cut above the Al gammadion. The top amino acid layers display large and

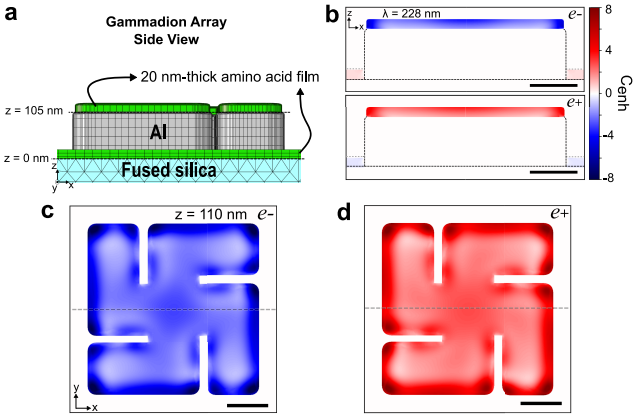

Figure 3. Near-field optical chirality calculations. (a) Gammadion array side view with reference point. (b−d) Near-field optical chirality enhancement of a LH gammadion coated with 20 nm of rac-Tyr illuminated at resonant frequency with CPL. The top amino acid layer experiences high and homogeneous values of C_{enh}. Furthermore, as we switch the CPL state (handedness) from negative (e^-) to positive ellipticity (e^+), C_{enh} flips in sign. Scale bar: 100 nm.

homogeneous values for C_{enh}, with good positional overlap with the enhancements in the electric field (Figure S7a,b). Conversely, the bottom Tyr layer displays small (Figure 3b) and inhomogeneous (Figure S8) values of C_{enh}, with electric field enhancements confined only to the gammadion perimeter (Figure S7c,d). We expect the plasmonic−molecular interactions from the top layer to primarily contribute to the observed results. Furthermore, if a nanostructure is to be utilized in enantiomeric discrimination, a desired characteristic is that its near-field C_{enh} flips in sign when alternating between the two circular polarizations.[5] From Figure 3c,d, the sign is clearly reversed, leading to a homogeneous difference in optical chirality enhancement;[5] i.e., $\Delta C_{enh} = C_{enh+} - C_{enh-}$ for the top amino acid layer (Figure S9).

To corroborate the results of the far-field EM simulations, we performed analogous experiments. We started by sublimating[32,58,59] 30 nm of tyrosine over lithographically defined Al gammadions. We characterize the samples with Mueller matrix (MM) polarimetry in transmission and retrieve the chiroptical signals with an analytic inversion of the MM[60] (see Supporting Information for detailed sample fabrication and optical characterization). This avoids potential artifacts to the chiroptical signals arising from linear effects[61] from either the gammadion arrays or biomolecular films. The nanostructures without any biomolecular coating display optical activity from the far-UV ($\lambda <$ 250 nm) to the visible part of the spectrum (Figure S11b,c). The fabricated gammadions have arms with width of ∼150 nm, ∼15 nm of gap between adjacent arms, and periodicity of 600 nm (see Figure S11d,e for SEM micrographs). To allow a reliable comparison between each amino acid film (L-, D-, or rac-Tyr), we used the same gammadion arrays throughout the experiments. We removed the tyrosine coatings by immersing the sample in dimethylformamide (DMF)[62] for 15 min with gentle agitation, followed by a DMF and IPA rinse and N_2 drying. We kept track of the chiroptical signals of the bare arrays before each biomolecular deposition step. We did not observe changes in the CD or CB signals of the bare samples after cleaning them with DMF (Figure S12).

Panels a and b of Figure 4 show the CD and CB signals of 30 nm-thick films of L-, D-, and rac-Tyr (see Figure S13 for

https://doi.org/10.1021/acs.nanolett.2c01724
Nano Lett. 2022, 22, 7343−7350

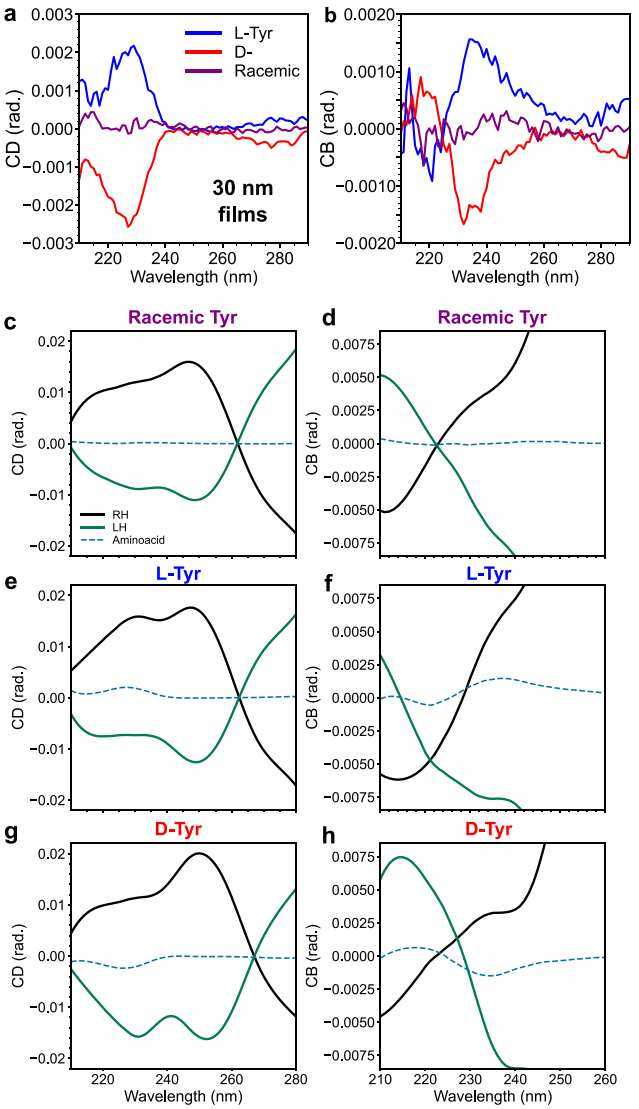

Figure 4. Experimental results of the plasmonic-biomolecular system. (a) CD and (b) CB of 30 nm thick films of L-, D-, and *rac*-tyrosine on top of a fused-silica substrate. The CD and CB peaks previously obtained for the 90 nm L-Tyr film are still observable, although the CB signal is relatively noisy, especially for the peak at ∼218 nm. CD and CB spectra of the bare amino acid films and the Al gammadion arrays coated with (c, d) rac-Tyr, (e, f) L-Tyr, and (g, h) D-Tyr. (c, d) When the nanostructures are surrounded by racemic layers, the CD (c) and CB (d) spectra of the coated gammadion enantiomorphs display good mirror symmetry. Perfect mirror symmetry is limited by nanofabrication heterogeneities. (e−h) Conversely, when the films are chiral, the mirror symmetry is lost, as also observed on the simulations. These effects go beyond an additive effect. The perturbations arising from the chirality of the biomolecular film can be used to determine its handedness.

their extinction spectra). The spectral features previously obtained for the thick L-Tyr film (Figure 2a,b) are still resolved, i.e., CD peak at 228 nm and CB peaks at 218 and 237 nm. This was expected because of the low thickness (<100 nm) of the amino acid films.[58] When the arrays are coated with rac-Tyr, the CD and CB of the RH and LH nanostructures display good mirror symmetry (Figure 4c,d). Conversely, the handed amino acid films (L- or D-Tyr) notably perturb the chiroptical signals of the gammadions enantiomorphs. As shown in Figure 4e−h, the CD and CB of RH and LH nanostructures coated with L- or D-Tyr lose their spectral mirror image. The most pronounced features are the intense peaks appearing at $\lambda \approx 228$ nm in the CD spectra of the RH gammadion coated with L-Tyr and of the LH gammadion coated with D-Tyr (Figure 4e,g). Simultaneously, the CD signals for the other gammadion−amino acid combinations are relatively flat in this region, due to the opposite signs of the plasmonic and amino acid CD. At longer wavelengths, where the chiral amino acid films have vanishing OA, the chiroptical signals of the RH and LH gammadions are essentially mirror-symmetric, regardless of the amino acid handedness or lack thereof (Figure S14). These results are consistent with the numerical calculations. Here, we do not perform any spectral summations of the chiroptical signals from the gammadion enantiomers in order to avoid data postprocessing, previously criticized due to the heterogeneities of nanofabricated chiral samples. Instead, we envision a platform where enantiomeric discrimination is enabled by fingerprint-like perturbations to the chiroptical signal of the system, which will depend on the overlap of plasmonic and biomolecular chiral resonances. Nevertheless, to show that the effects in Figure 4e−h go beyond an additive effect, we subtracted the corresponding CD or CB signals of the bare chiral Tyr film from the chiroptical signals of the chiral Tyr coated gammadion enantiomers (Figure S15).

One desirability of plasmonic biosensors is the amplification of weak signals and the detection of small quantities of analyte.[63] Therefore, we shifted to evaporate ultrathin (average of 9.4 nm in thickness) films of Tyr, for which the CD spectra were barely resolved, and the CB signal could not be reliably determined in our polarimeter (Figure S16). We estimate the quantity of Tyr to be on the order of ∼10 attomol/(unit cell). Here, we focused on the CB signals of the system, given that the gammadion arrays did not display strong CD peaks at the region of interest (Figure S17). Panels a−c of Figure 5 present the CB spectra of the RH and LH gammadion arrays coated with rac-, L-, and D-Tyr films, respectively. For plots with each amino acid, we also included a reference CB spectrum of a thick film to aid in the visualization of the molecular OA signals (or lack thereof). Clearly, the chiral nanostructures interact differently with the handed amino acids compared to when the gammadions are coated with a racemic film. Again, following the preceding theoretical and experimental results, these variations are pronounced in the biomolecular chiral resonance region, specifically at $\lambda \approx 240$ nm where there is a good overlap between the plasmonic and molecular CB peaks.

To further understand the effects of plasmonic−biomolecular OA spectral overlap, we scaled the unit cell of the fabricated arrays by factors of 7/8 and 9/8 (Figure 5d−i), intentionally altering the spectra of the bare gammadions. Panels d−f of Figure 5 present the CB spectra of the smallest gammadion arrays (e.g., 7/8 scaled) coated with rac-, L-, and D-Tyr films, respectively. When compared to the CB signal of the RH nanostructures coated with a racemic film, the spectrum of the same array coated with L-Tyr (Figure 5e) displays a distinct concavity for $\lambda < 230$ nm (blue markers), due to the relative amplitudes and opposing signs of the plasmonic and biomolecular OA spectra in this wavelength regime. Furthermore, a distinct peak appears at $\lambda \approx 237$ nm (blue arrow). Similar results were obtained for the LH gammadions and D-Tyr combination (Figure 5f), effectively permitting the arrays to be used for enantiomeric discrimination. For the

https://doi.org/10.1021/acs.nanolett.2c01724
Nano Lett. 2022, 22, 7343−7350

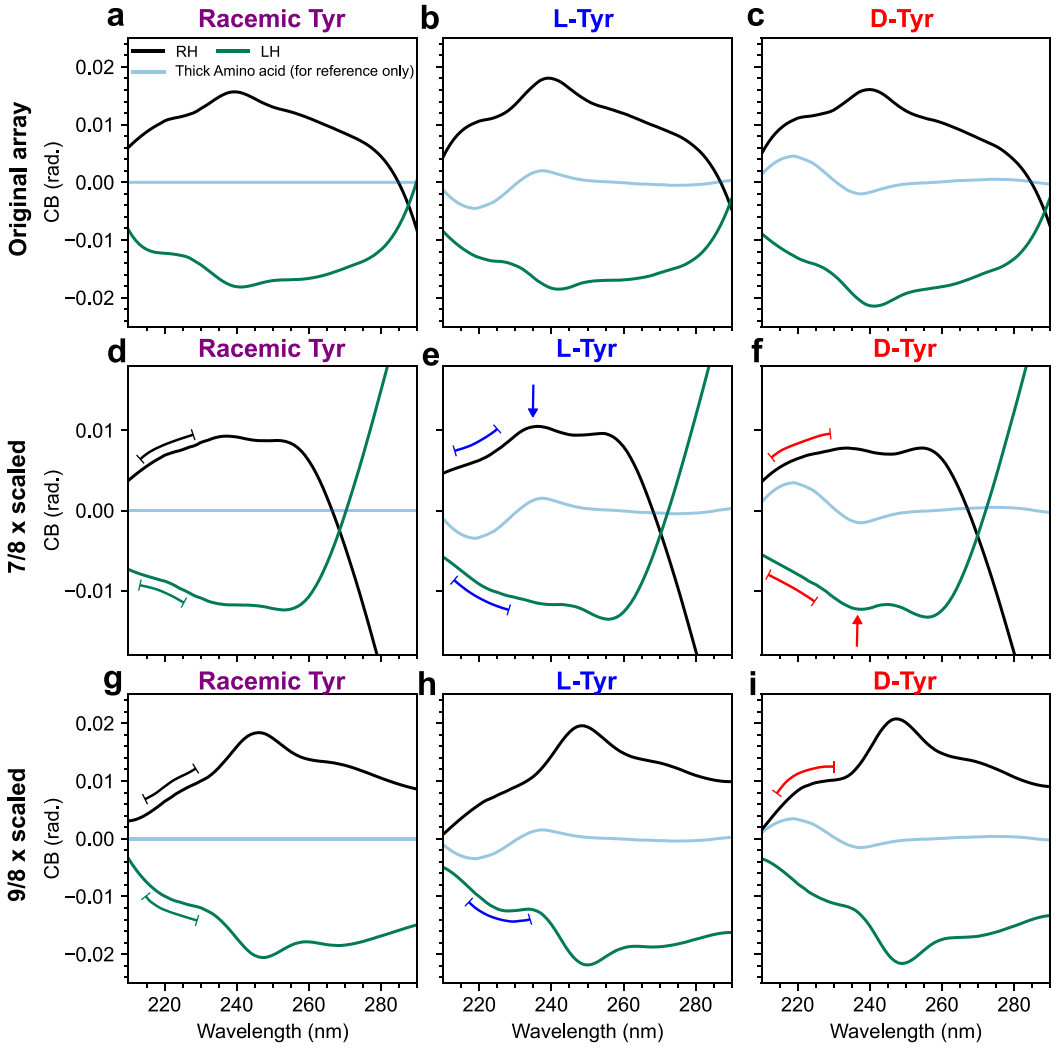

Figure 5. Experimental CB of the plasmonic−biomolecular system ultrathin (<10 nm) films of (a) rac-Tyr, (b) L-Tyr, and (c) D-Tyr films deposited on the gammadion array. Note the CB peaks for the bare films are not reliably determined in our instrument. A reference CB spectrum for a thick Tyr film is shown in light blue. When the nanostructures are surrounded by rac-Tyr the CB (a) spectra of the gammadion enantiomorphs display good mirror symmetry. Note, that perfect mirror symmetry is limited by nanofabrication heterogeneities in the gammadion. (b, c) Conversely, when (b) L-Tyr or (c) D-Tyr films are deposited on the gammadions, the resulting left- and right-handed CB spectra show clear differences near the peaks of the (light blue) thick Tyr reference spectra. (d−f, g−i) CB results for 7/8 and 9/8 scaled gammadion arrays, with 9 nm of (d, g) rac-Tyr, (e, h) L-Tyr, and (f, i) D-Tyr films, respectively, displaying similar trends.

largest gammadion array (Figure 5g−i), the noticeable differences with respect to the control experiment (Figure 5g) were in the concavities of the CB (blue and red markers) spectra of the gammadions coated with chiral films for $\lambda < 237$ nm (Figure 5h,i). We reproduced the results of Figure 5d−i in eight sets of measurements for each amino acid (Figure S18). Furthermore, as predicted in the numerical calculations, at longer wavelengths where biomolecular OA is vanishing, we see no differences in the CB spectra of a gammadion array (i.e., RH) coated with rac-, L-, or D-Tyr (Figure S19).

In summary, we have shown that Al plasmonic nanostructures with far-ultraviolet chiroptical response can provide enantiomeric discrimination of ultrathin amino acid films. The unenhanced signals from the bare films (i.e., on top of the fused-silica substrate) were within the noise level of our instrument. This enhanced chiral biosensing is enabled by resonant interactions between chiral biomolecules and chiral plasmonic near-fields. Our simulated and experimental results confirm that the spectral overlap between plasmonic and natural OA is of great importance for enhanced biosensing. By evaporating ultrathin films (<10 nm) of tyrosine on the nanostructures, we show that minute quantities of biomolecules can perturb the plasmonic chiroptical signal and enable enantiomeric discrimination. The chiral signature of the plasmonic−biomolecular system strongly depends on how the resonances of these two components overlay on one another.

■ ASSOCIATED CONTENT

Supporting Information

The Supporting Information is available free of charge at https://pubs.acs.org/doi/10.1021/acs.nanolett.2c01724.

Experimental section with electromagnetic simulations, chiroptical characterization, chirality parameter retrieval, sample fabrication, and optical properties; electromagnetic simulations figures including simulated chirop-

https://doi.org/10.1021/acs.nanolett.2c01724
Nano Lett. 2022, 22, 7343−7350

tical signals and electric-field and optical chirality enhancements; experimental figures including chiroptical signals, SEM micrographs, extinction spectra, CD and CB spectra, and reproducibility study (PDF)

Refractive index and chirality parameter of L-Tyr (TXT)

AUTHOR INFORMATION

Corresponding Author

Kevin M. McPeak − *Gordon and Mary Cain Department of Chemical Engineering, Louisiana State University, Baton Rouge, Louisiana 70803, United States;* orcid.org/0000-0002-2766-104X; Email: kmcpeak@lsu.edu

Authors

Tiago Ramos Leite − *Gordon and Mary Cain Department of Chemical Engineering, Louisiana State University, Baton Rouge, Louisiana 70803, United States;* orcid.org/0000-0002-1491-807X

Lin Zschiedrich − *JCMwave GmbH, 14050 Berlin, Germany; Zuse Institute Berlin, 14195 Berlin, Germany*

Orhan Kizilkaya − *Louisiana State University Center for Advanced Microstructures and Devices, Baton Rouge, Louisiana 70806, United States*

Complete contact information is available at: https://pubs.acs.org/10.1021/acs.nanolett.2c01724

Author Contributions

K.M.M. and T.R.L. conceived the idea. T.R.L. fabricated the plasmonic arrays, measured their chiroptical response, and performed the electromagnetic simulations. L.Z. implemented the bi-isotropic model. T.R.L and O.K. deposited the amino acid thin films. T.R.L. wrote the manuscript with contributions from all coauthors. K.M.M. supervised and edited the manuscript. All authors have given approval to the final version of the manuscript.

Notes

The authors declare no competing financial interest.

ACKNOWLEDGMENTS

K.M.M. and T.R.L. are supported by the National Science Foundation CAREER Award No. 1653705. For the numerical implementation of the bi-isotropic model, this project has received funding from the European Metrology Programme for Innovation and Research (EMPIR), cofinanced by the participating States and from the European Union's Horizon 2020 research and innovation programme (Project 20FUN02 "POLIGHT") and from the German Federal Ministry of Education and Research (BMBF Forschungscampus MODAL, Project No. 05M20ZBM).

REFERENCES

(1) Tang, Y.; Cohen, A. E. Optical Chirality and Its Interaction with Matter. *Phys. Rev. Lett.* **2010**, *104* (16), 163901.

(2) Tang, Y.; Cohen, A. E. Enhanced Enantioselectivity in Excitation of Chiral Molecules by Superchiral Light. *Science* **2011**, *332* (6027), 333−336.

(3) Silverman, M. P.; Badoz, J. Interferometric Enhancement of Chiral Asymmetries: Ellipsometry with an Optically Active Fabry−Perot Interferometer. *J. Opt. Soc. Am. A* **1994**, *11* (6), 1894−1917.

(4) Barron, L. D. *Molecular Light Scattering and Optical Activity*, 2nd ed., rev.enl.; Cambridge University Press: Cambridge, UK; New York, 2004; pp 1−10.

(5) Schäferling, M.; Dregely, D.; Hentschel, M.; Giessen, H. Tailoring Enhanced Optical Chirality: Design Principles for Chiral Plasmonic Nanostructures. *Phys. Rev. X* **2012**, *2* (3), 031010.

(6) Hentschel, M.; Schäferling, M.; Duan, X.; Giessen, H.; Liu, N. Chiral Plasmonics. *Sci. Adv.* **2017**, *3* (5), e1602735.

(7) Warning, L. A.; Miandashti, A. R.; McCarthy, L. A.; Zhang, Q.; Landes, C. F.; Link, S. Nanophotonic Approaches for Chirality Sensing. *ACS Nano* **2021**, *15* (10), 15538−15566.

(8) Vestler, D.; Ben-Moshe, A.; Markovich, G. Enhancement of Circular Dichroism of a Chiral Material by Dielectric Nanospheres. *J. Phys. Chem. C* **2019**, *123* (8), 5017−5022.

(9) Zhao, X.; Reinhard, B. M. Switchable Chiroptical Hot-Spots in Silicon Nanodisk Dimers. *ACS Photonics* **2019**, *6* (8), 1981−1989.

(10) García-Guirado, J.; Svedendahl, M.; Puigdollers, J.; Quidant, R. Enhanced Chiral Sensing with Dielectric Nanoresonators. *Nano Lett.* **2020**, *20* (1), 585−591.

(11) Solomon, M. L.; Abendroth, J. M.; Poulikakos, L. V.; Hu, J.; Dionne, J. A. Fluorescence-Detected Circular Dichroism of a Chiral Molecular Monolayer with Dielectric Metasurfaces. *J. Am. Chem. Soc.* **2020**, *142* (43), 18304−18309.

(12) Solomon, M. L.; Saleh, A. A. E.; Poulikakos, L. V.; Abendroth, J. M.; Tadesse, L. F.; Dionne, J. A. Nanophotonic Platforms for Chiral Sensing and Separation. *Acc. Chem. Res.* **2020**, *53* (3), 588−598.

(13) Berova, N., Nakanishi, K., Woody, R. *Circular Dichroism: Principles and Applications*, 2nd ed.; Wiley-VCH: New York, 2000; pp 601−613.

(14) Huang, K.; Deng, J.; Leong, H. S.; Yap, S. L. K.; Yang, R. B.; Teng, J.; Liu, H. Ultraviolet Metasurfaces of ≈80% Efficiency with Antiferromagnetic Resonances for Optical Vectorial Anti-Counterfeiting. *Laser Photonics Rev.* **2019**, *13* (5), 1800289.

(15) Zhang, C.; Divitt, S.; Fan, Q.; Zhu, W.; Agrawal, A.; Lu, Y.; Xu, T.; Lezec, H. J. Low-Loss Metasurface Optics down to the Deep Ultraviolet Region. *Light Sci. Appl.* **2020**, *9* (1), 55.

(16) Hu, J.; Lawrence, M.; Dionne, J. A. High Quality Factor Dielectric Metasurfaces for Ultraviolet Circular Dichroism Spectroscopy. *ACS Photonics* **2020**, *7* (1), 36−42.

(17) Kim, T.; Park, Q.-H. Molecular Chirality Detection Using Plasmonic and Dielectric Nanoparticles. *Nanophotonics* **2022**, *11* (9), 1897−1904.

(18) Chen, W.; Bian, A.; Agarwal, A.; Liu, L.; Shen, H.; Wang, L.; Xu, C.; Kotov, N. A. Nanoparticle Superstructures Made by Polymerase Chain Reaction: Collective Interactions of Nanoparticles and a New Principle for Chiral Materials. *Nano Lett.* **2009**, *9* (5), 2153−2159.

(19) Kuzyk, A.; Schreiber, R.; Fan, Z.; Pardatscher, G.; Roller, E.-M.; Högele, A.; Simmel, F. C.; Govorov, A. O.; Liedl, T. DNA-Based Self-Assembly of Chiral Plasmonic Nanostructures with Tailored Optical Response. *Nature* **2012**, *483* (7389), 311−314.

(20) Ma, W.; Xu, L.; de Moura, A. F.; Wu, X.; Kuang, H.; Xu, C.; Kotov, N. A. Chiral Inorganic Nanostructures. *Chem. Rev.* **2017**, *117* (12), 8041−8093.

(21) Song, C.; Blaber, M. G.; Zhao, G.; Zhang, P.; Fry, H. C.; Schatz, G. C.; Rosi, N. L. Tailorable Plasmonic Circular Dichroism Properties of Helical Nanoparticle Superstructures. *Nano Lett.* **2013**, *13* (7), 3256−3261.

(22) Wang, L.-Y.; Smith, K. W.; Dominguez-Medina, S.; Moody, N.; Olson, J. M.; Zhang, H.; Chang, W.-S.; Kotov, N.; Link, S. Circular Differential Scattering of Single Chiral Self-Assembled Gold Nanorod Dimers. *ACS Photonics* **2015**, *2* (11), 1602−1610.

(23) Smith, K. W.; Zhao, H.; Zhang, H.; Sánchez-Iglesias, A.; Grzelczak, M.; Wang, Y.; Chang, W.-S.; Nordlander, P.; Liz-Marzán, L. M.; Link, S. Chiral and Achiral Nanodumbbell Dimers: The Effect of Geometry on Plasmonic Properties. *ACS Nano* **2016**, *10* (6), 6180−6188.

(24) Fan, Z.; Govorov, A. O. Plasmonic Circular Dichroism of Chiral Metal Nanoparticle Assemblies. *Nano Lett.* **2010**, *10* (7), 2580−2587.

(25) Govorov, A. O.; Fan, Z.; Hernandez, P.; Slocik, J. M.; Naik, R. R. Theory of Circular Dichroism of Nanomaterials Comprising Chiral

Molecules and Nanocrystals: Plasmon Enhancement, Dipole Interactions, and Dielectric Effects. *Nano Lett.* **2010**, *10* (4), 1374−1382.
(26) Slocik, J. M.; Govorov, A. O.; Naik, R. R. Plasmonic Circular Dichroism of Peptide-Functionalized Gold Nanoparticles. *Nano Lett.* **2011**, *11* (2), 701−705.
(27) Maoz, B. M.; Chaikin, Y.; Tesler, A. B.; Bar Elli, O.; Fan, Z.; Govorov, A. O.; Markovich, G. Amplification of Chiroptical Activity of Chiral Biomolecules by Surface Plasmons. *Nano Lett.* **2013**, *13* (3), 1203−1209.
(28) Kneer, L. M.; Roller, E.-M.; Besteiro, L. V.; Schreiber, R.; Govorov, A. O.; Liedl, T. Circular Dichroism of Chiral Molecules in DNA-Assembled Plasmonic Hotspots. *ACS Nano* **2018**, *12* (9), 9110−9115.
(29) Zhang, Q.; Hernandez, T.; Smith, K. W.; Hosseini Jebeli, S. A.; Dai, A. X.; Warning, L.; Baiyasi, R.; McCarthy, L. A.; Guo, H.; Chen, D.-H.; Dionne, J. A.; Landes, C. F.; Link, S. Unraveling the Origin of Chirality from Plasmonic Nanoparticle-Protein Complexes. *Science* **2019**, *365* (6460), 1475−1478.
(30) García-Etxarri, A.; Dionne, J. A. Surface-Enhanced Circular Dichroism Spectroscopy Mediated by Nonchiral Nanoantennas. *Phys. Rev. B* **2013**, *87* (23), 235409.
(31) Yoo, S.; Cho, M.; Park, Q.-H. Globally Enhanced Chiral Field Generation by Negative-Index Metamaterials. *Phys. Rev. B* **2014**, *89* (16), 161405.
(32) García-Guirado, J.; Svedendahl, M.; Puigdollers, J.; Quidant, R. Enantiomer-Selective Molecular Sensing Using Racemic Nanoplasmonic Arrays. *Nano Lett.* **2018**, *18* (10), 6279−6285.
(33) Yoo, S.; Park, Q.-H. Metamaterials and Chiral Sensing: A Review of Fundamentals and Applications. *Nanophotonics* **2019**, *8* (2), 249−261.
(34) Schäferling, M.; Yin, X.; Engheta, N.; Giessen, H. Helical Plasmonic Nanostructures as Prototypical Chiral Near-Field Sources. *ACS Photonics* **2014**, *1* (6), 530−537.
(35) Hendry, E.; Carpy, T.; Johnston, J.; Popland, M.; Mikhaylovskiy, R. V.; Lapthorn, A. J.; Kelly, S. M.; Barron, L. D.; Gadegaard, N.; Kadodwala, M. Ultrasensitive Detection and Characterization of Biomolecules Using Superchiral Fields. *Nat. Nanotechnol.* **2010**, *5* (11), 783−787.
(36) Tullius, R.; Karimullah, A. S.; Rodier, M.; Fitzpatrick, B.; Gadegaard, N.; Barron, L. D.; Rotello, V. M.; Cooke, G.; Lapthorn, A.; Kadodwala, M. Superchiral" Spectroscopy: Detection of Protein Higher Order Hierarchical Structure with Chiral Plasmonic Nanostructures. *J. Am. Chem. Soc.* **2015**, *137* (26), 8380−8383.
(37) Zhao, Y.; Askarpour, A. N.; Sun, L.; Shi, J.; Li, X.; Alù, A. Chirality Detection of Enantiomers Using Twisted Optical Metamaterials. *Nat. Commun.* **2017**, *8* (1), 14180.
(38) Lee, S.; Yoo, S.; Park, Q.-H. Microscopic Origin of Surface-Enhanced Circular Dichroism. *ACS Photonics* **2017**, *4* (8), 2047−2052.
(39) Besteiro, L. V.; Zhang, H.; Plain, J.; Markovich, G.; Wang, Z.; Govorov, A. O. Aluminum Nanoparticles with Hot Spots for Plasmon-Induced Circular Dichroism of Chiral Molecules in the UV Spectral Interval. *Adv. Opt. Mater.* **2017**, *5* (16), 1700069.
(40) Lan, X.; Zhou, X.; McCarthy, L. A.; Govorov, A. O.; Liu, Y.; Link, S. DNA-Enabled Chiral Gold Nanoparticle−Chromophore Hybrid Structure with Resonant Plasmon−Exciton Coupling Gives Unusual and Strong Circular Dichroism. *J. Am. Chem. Soc.* **2019**, *141* (49), 19336−19341.
(41) Nordén, B.; Tjerneld, F. Structure of methylene blue−DNA complexes studied by linear and circular dichroism spectroscopy. *Biopolymers* **1982**, *21* (9), 1713−1734.
(42) Allenmark, S. Induced Circular Dichroism by Chiral Molecular Interaction. *Chirality* **2003**, *15* (5), 409−422.
(43) Jha, S. K.; Ahmed, Z.; Agio, M.; Ekinci, Y.; Löffler, J. F. Deep-UV Surface-Enhanced Resonance Raman Scattering of Adenine on Aluminum Nanoparticle Arrays. *J. Am. Chem. Soc.* **2012**, *134* (4), 1966−1969.
(44) Knight, M. W.; King, N. S.; Liu, L.; Everitt, H. O.; Nordlander, P.; Halas, N. J. Aluminum for Plasmonics. *ACS Nano* **2014**, *8* (1), 834−840.
(45) McPeak, K. M.; van Engers, C. D.; Bianchi, S.; Rossinelli, A.; Poulikakos, L. V.; Bernard, L.; Herrmann, S.; Kim, D. K.; Burger, S.; Blome, M.; Jayanti, S. V.; Norris, D. J. Ultraviolet Plasmonic Chirality from Colloidal Aluminum Nanoparticles Exhibiting Charge-Selective Protein Detection. *Adv. Mater.* **2015**, *27* (40), 6244−6250.
(46) McPeak, K. M.; Jayanti, S. V.; Kress, S. J. P.; Meyer, S.; Iotti, S.; Rossinelli, A.; Norris, D. J. Plasmonic Films Can Easily Be Better: Rules and Recipes. *ACS Photonics* **2015**, *2* (3), 326−333.
(47) McClain, M. J.; Schlather, A. E.; Ringe, E.; King, N. S.; Liu, L.; Manjavacas, A.; Knight, M. W.; Kumar, I.; Whitmire, K. H.; Everitt, H. O.; Nordlander, P.; Halas, N. J. Aluminum Nanocrystals. *Nano Lett.* **2015**, *15* (4), 2751−2755.
(48) Sihvola, A. H.; Viitanen, A. J.; Lindell, I. V. *Electromagnetic Waves in Chiral and Bi-Isotropic Media*; Artech House: Boston, 1994; pp 1−18.
(49) Semchenko, I.; Serdyukov, A.; Sihvola, A.; Tretyakov, S. *Electromagnetics of Bi-anisotropic Materials: Theory and Applications*; Electrocomponent Science Monographs; Gordon and Breach: Amsterdam, 2001; pp 28−29.
(50) Zhao, R.; Koschny, T.; Soukoulis, C. M. Chiral Metamaterials: Retrieval of the Effective Parameters with and without Substrate. *Opt. Express* **2010**, *18* (14), 14553−14567.
(51) Oh, S. S.; Hess, O. Chiral Metamaterials: Enhancement and Control of Optical Activity and Circular Dichroism. *Nano Converg.* **2015**, *2* (1), 24.
(52) Mohammadi, E.; Tsakmakidis, K. L.; Askarpour, A. N.; Dehkhoda, P.; Tavakoli, A.; Altug, H. Nanophotonic Platforms for Enhanced Chiral Sensing. *ACS Photonics* **2018**, *5* (7), 2669−2675.
(53) Both, S.; Schäferling, M.; Sterl, F.; Muljarov, E. A.; Giessen, H.; Weiss, T. Nanophotonic Chiral Sensing: How Does It Actually Work? *ACS Nano* **2022**, *16* (2), 2822−2832.
(54) Kelly, S. M.; Jess, T. J.; Price, N. C. How to Study Proteins by Circular Dichroism. *Biochim. Biophys. Acta BBA - Proteins Proteomics* **2005**, *1751* (2), 119−139.
(55) Krittanai, C.; Johnson, W. C. Correcting the Circular Dichroism Spectra of Peptides for Contributions of Absorbing Side Chains. *Anal. Biochem.* **1997**, *253* (1), 57−64.
(56) Lan, X.; Zhou, X.; McCarthy, L. A.; Govorov, A. O.; Liu, Y.; Link, S. DNA-Enabled Chiral Gold Nanoparticle−Chromophore Hybrid Structure with Resonant Plasmon−Exciton Coupling Gives Unusual and Strong Circular Dichroism. *J. Am. Chem. Soc.* **2019**, *141* (49), 19336−19341.
(57) Nesterov, M. L.; Yin, X.; Schäferling, M.; Giessen, H.; Weiss, T. The Role of Plasmon-Generated Near Fields for Enhanced Circular Dichroism Spectroscopy. *ACS Photonics* **2016**, *3* (4), 578−583.
(58) Tanaka, M.; Kodama, Y.; Nakagawa, K. Circular Dichroism of Amino Acid Films in UV-VUV Region. *Enantiomer* **2002**, *7* (4−5), 185−190.
(59) Takahashi, J.; Shinojima, H.; Seyama, M.; Ueno, Y.; Kaneko, T.; Kobayashi, K.; Mita, H.; Adachi, M.; Hosaka, M.; Katoh, M. Chirality Emergence in Thin Solid Films of Amino Acids by Polarized Light from Synchrotron Radiation and Free Electron Laser. *Int. J. Mol. Sci.* **2009**, *10* (7), 3044−3064.
(60) Arteaga, O.; Canillas, A. Analytic Inversion of the Mueller-Jones Polarization Matrices for Homogeneous Media. *Opt. Lett.* **2010**, *35* (4), 559−561.
(61) Arteaga, O.; Kahr, B. Mueller Matrix Polarimetry of Bianisotropic Materials. *J. Opt. Soc. Am. B* **2019**, *36* (8), F72.
(62) Li, X.; Li, K.; Farajtabar, A.; He, Y.; Chen, G.; Zhao, H. Solubility of D-Tryptophan and L-Tyrosine in Several Organic Solvents: Determination and Solvent Effect. *J. Chem. Eng. Data* **2019**, *64* (7), 3164−3169.
(63) Mejía-Salazar, J. R.; Oliveira, O. N. Plasmonic Biosensing. *Chem. Rev.* **2018**, *118* (20), 10617−10625.

https://doi.org/10.1021/acs.nanolett.2c01724
Nano Lett. 2022, 22, 7343−7350